ENGINEERING RESEARCH JOURNAL (ERJ)
Vol. 1, No. 48 Apr. 2021, pp 189-203
Journal Homepage: http://erj.bu.edu.eg

ROBUST WRIST VEINS ROI LOCALIZATION ALGORITHM BASED ON AN IMPROVED JOINT-ENTROPY THRESHOLDING METHOD

Abdelwahab Al-Sammak[1], May Salama[2], Sarah Moustafa kamel[3]

Faculty of Engineering, Shoubra
Benha University
Email[1]: asammak@feng.bu.edu.eg
Email[2]: msalama@megacom-int.com
Email[3]: sara.kamel@feng.bu.edu.eg

ABSTRACT

Hand veins, being an inner body trait, demonstrated a reliable, secure and anti-spoofing biometric trait. Vein recognition performance highly depends on the precise detection of the vein Region-of-Interest (ROI). External influences like poor illumination, noise, blurring, complicated backgrounds, and incomplete capturing of hand region can affect the quality while capturing, causing performance degradation of wrist region segmentation that eventually leads to inaccurate ROI detection. In this paper, we propose a ROI localization method for wrist veins images. It consists of three steps: wrist region segmentation based on joint-entropy (JE) thresholding method, wrist orientation correction and ROI detection. The proposed segmentation method is compared with fifteen image segmentation methods using low quality wrist-vein images from PUT vein dataset and is evaluated by six segmentation evaluation metrics. Experiments show that the proposed method produced 99.524% accuracy that is 1.022% more accurate than the original JE thresholding method.

KEYWORDS: wrist veins, image segmentation, Joint Entropy thresholding, ROI localization.

1. INTRODUCTION

Recently, biometric-based recognition technologies prevail most of individual recognition systems. One of the strongest biometrics is the hand veins pattern because of its universality, stability and uniqueness even for identical twins [1]. Comparing with other biometrics, veins are resistant against spoofing because they are inner features of the human body and can be clearly visible only under a specific spectral range of infrared light [2], while palm-print, fingerprint, face or hand geometry traits are liable to be copied, forged and simulated because they are outer features. In addition, the vein image acquisition technologies, whether by using far-infrared (FIR) imaging or near-infrared (NIR) imaging, depend on alive body characteristics [2], which makes it possible to distinguish between real-live and fake vein images [3-4]. Although EEG signals are also robust against spoofing, acquiring EEG signals is not an easy task because it has to be done with headset, in an absolutely quiet room. Hand veins capturing process is more user convenient due to its direct presence underneath the superficial skin, thus it can be easily captured using an inexpensive infrared camera. Hence, hand veins have become a reliable, secure and accurate biometric trait.

Hand veins are divided into four types used for identity recognition: hand dorsum veins,

palm veins, finger veins, and wrist veins patterns. Wrist-veins were chosen to be the scope of this paper, as it was noted that there is deficiency in researches using wrist veins pattern in identity recognition. The raw vein image usually contains portions, with useless information, other than the wrist region. Thus, the first step in vein recognition systems is the ROI detection that aims to detect only the most informative region in the image and remove all unwanted details, in order to efficiently perform and speed up the subsequent steps of the vein recognition system.

Unfortunately, some external influences can easily affect the quality of acquired images such as poor illumination, noise, blurring, shadows or complicated backgrounds. Moreover, hand posture variations due to allowing freely hand positioning during the image acquisition process can lead to incomplete capturing of the hand region. All these factors can lead to inaccurate ROI detection, which in turn results in declining the performance of recognition systems.

In this paper, we propose an integrated wrist-vein ROI localization approach consisting of a wrist region segmentation method that is robust to most of the mentioned factors, followed by wrist orientation correction and ROI detection. Figure 1 shows the three steps of the proposed methodology. Firstly, noisy regions in the image background are eliminated in order to guarantee purity of the gray level co-occurrence matrix (GLCM) of the image. This is followed by applying the joint-entropy thresholding algorithm to compute the appropriate threshold value. Secondly, wrist orientation correction step is applied to correct any rotations caused during capturing. Finally, the ROI detection step which aims to localize the smallest possible rectangular region that can contain the whole wrist region. It is worth noting that extracting aligned ROIs for different wrist-vein images is not the goal of the proposed approach, since translation and scale corrections are not of importance as they can be resolved by using invariant features for vein recognition. Only wrist orientation correction process is considered in order to support accurately localizing the smallest possible rectangle containing the wrist region.

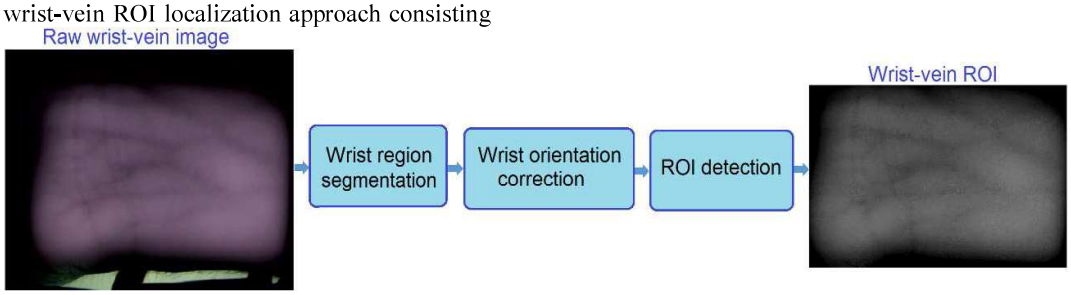

Fig 1 Framework of the wrist vein ROI localization methodology

The rest of the paper is structured as follows: the next section lists the related work. Section II presents the related work of vein localization methods. Section III describes the proposed wrist-vein ROI detection algorithm while section IV demonstrates and discusses the results. Finally, section V concludes the paper with a summary of the proposed approach along with an outlook for the future work.

2. RELATED WORK

During hand region localization step, the hand region in the captured image must be detected and separated from the background by using one of the following image segmentation techniques: edge-based segmentation, threshold-based segmentation, region-based segmentation and clustering-based segmentation.

In [5-7], an edge-based segmentation technique was used for finger region localization by detecting its boundary. By assuming that the boundary between the finger and the background has the sharpest edges in the image, it can be detected by passing an edge detector mask on the whole image, then dividing the image into two halves and determining the highest response point for each column at each half. This technique is not robust against the incomplete capturing of the finger region and the complicated backgrounds [8]. It also fails when its main assumption is unsatisfied due to existence of some weak finger edges or other edges in the image sharper than the finger edges. Moreover, the finger region supposed to be almost around the middle of the acquired image in order to have a part of its boundary at each image half.

Another hand region detection method is applying an edge detector on the image in order to detect its edges, such as Sobel edge detector as in [9-10] or Canny edge detector as in [11-12], followed by a post-processing step for connecting the broken hand edges using the morphological closing operation, then filling these edges so as to obtain solid regions. Although its simplicity, this method is not robust against the complicated background since any unwanted background details close to the hand region can be associated to it due to the usage of closing operation. It is also sensitive to the sharpness of the hand edges, since the existence of weak hand edges can result in large breaks in the hand contour that need a much bigger structural element to connect them. So, it is a tradeoff between connecting the broken hand edges and avoiding connecting the unwanted background details with it.

Otsu thresholding method is the most used segmentation method for hand region localization in vein images [13-15]. It is a clustering-based image thresholding method that depends only on the image's intensity histogram, assuming to be a bimodal histogram with a sharp deep valley separating its two peaks. Moreover, the relative size of background and object regions in the image must be close to each other in order to satisfy the histogram bimodality. In spite of its speed, the segmentation results can be of low quality if the bimodal histogram assumption isn't satisfied. Therefore, it is highly sensitive to uneven illumination, noise, shadows, and reflection problems that can easily occur during the image capturing. Existence of one of these factors in an image affects its histogram shape; causing it to lose its bimodality. Moreover, it depends only on the intensity histogram of the image, ignoring its inter-pixel spatial relationships. This leads to producing the same threshold value for different images with exactly similar histograms [16], and also does not ensure interconnected segmented regions.

In [17-18], the unsupervised K-means clustering algorithm has been used to segment the hand region from the background by clustering the gray-level samples in the image into two classes, assuming that the image consisting of only the background and hand regions. The drawbacks of this method are the difficulty of predicting a fixed-k for all images, and its ability to work only with spherical clusters. Moreover, segmentation results are un-stable and highly sensitive to the user-defined clusters number and their randomly selected initial centroids, since the final clustering can significantly vary through several runs of the algorithm due to the changes of the initial cluster centers. Furthermore, the random selection of initial centroids may cause the algorithm to stick into local minima [19]. A solution for this is to repeat clustering several times using different initial centroids and retain only the best segmentation result, which is very time consuming. Table 1 summarizes the advantages and disadvantages of the above listed methods.

Table 1 Comparison between various image segmentation methods commonly used for localizing hand vein ROI in NIR images.

Image segmentation method	Strength points	Weakness points
Lee's finger region localization [5-7]	• Works well for image with high contrast between its regions. • Fast and simple	High sensitivity to: • incomplete capturing of finger region • complicated backgrounds • sharpness of the finger edges • existence of other edges in the image sharper than the finger edges • location of the finger region in the acquired image
Sobel [9-10] and Canny [11-12] edge detectors	• Works well for image with high contrast between its regions. • Fast and simple	• Sensitivity to sharpness of the hand edges • difficulty of selecting the proper structural element size for the closing operation • tends to connect objects close to each other • cannot distinguish between regions that are not well separated from each

		other
Otsu global thresholding [13-15]	• Does not need prior knowledge about the image • Computationally inexpensive • Fast and simple	• works well only for images with bimodal histograms • High sensitivity to uneven illumination, noise, shadows, and reflection problems • Ignoring the image's spatial information; leads to producing the same threshold value for different images with exactly similar histograms, and also does not ensure interconnected segmented regions.
K-means clustering [17-18]	• computationally fast for small number of clusters • works well for image whose regions are not well separated from each other	• High sensitivity to user-defined clusters number, in addition to the difficulty of predicting a fixed-k for all images • High sensitivity to randomly selected initial centroids; resulting in un-stable segmentation results • Liable to stick into local minima • Works well only with spherical clusters.

3. PROPOSED ALGORITHM

Thresholding is the most popular segmentation method because of its simplicity and speed. Unfortunately, the most common single global thresholding methods depend only on the intensity histogram that can be considered as a first-order statistic of the image regardless of its spatial information, in addition to the assumption of bimodal histogram that is hard to be always satisfied. All of these factors lead to many weaknesses as discussed in section 2. On the other hand, the Gray Level Co-occurrence Matrix (GLCM), proposed in [16], is a higher-order statistic of the image. It is defined as a 2D histogram of the gray-levels transitions between every two adjacent pixels in the image. Since the GLCM-based thresholding methods depend only on the GLCM of the image instead of its intensity histogram, they consider the spatial distributions of gray levels in the image during their threshold values computation.

The GLCM of a gray-scale image f of size M×N with gray levels in the range [0, 1. . . L-1] is an L×L square matrix denoted by $T = [t_{ij}]_{L\times L}$, where t_{ij} is the $(i,j)^{th}$ element of co-occurrence matrix that defines the number of occurrences of the gray transition from the gray level i to the gray level j between pair of adjacent pixels in the image by considering only the horizontally right and vertically lower transitions. Figure 2 shows an example of wrist image with different views of its GLCM.

$$t_{ij} = \sum_{l=1}^{M} \sum_{k=1}^{N} \delta(l,k) \qquad 1)$$

$$\delta(l,k) = \begin{cases} 1 \ if \begin{cases} f(l,k) = i \ and \ f(l,k+1) = j \\ f(l,k) = i \ and \ f(l+1,k) = j \end{cases} \\ 0 \ otherwise \end{cases} \qquad 2)$$

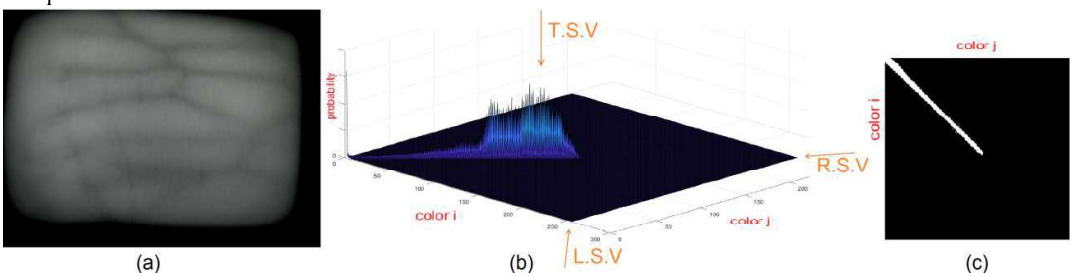

Fig 2 (a) wrist image, (b) 3D graph of GLCM, (c) top side view of 3D GLCM graph.

By analyzing the general structure of co-occurrence matrix, we have found that all the gray transitions along each k^{th} diagonal line have an equal Standard Deviation (SD) value that is symmetric around the primary diagonal line ($k = 0$). Moreover, the primary diagonal line has zero-valued SD for all its gray transitions. The farther the k^{th} diagonal line becomes from the primary diagonal, the higher the SD value it will have along all its gray transitions, as shown in figure 3(a).

Let S to be the determined threshold value for segmenting the image into foreground and background, in a way that the higher gray levels belong to the foreground region, while the lower gray levels belong to the background region. The GLCM is divided into four quadrants that are categorized into two types. A and C quadrants are the local quadrants that hold the local transitions inside background and foreground respectively, while B and D are the joint quadrants that hold the joint transitions from background to foreground and from foreground to background respectively, as shown in figure 3(b) [16].

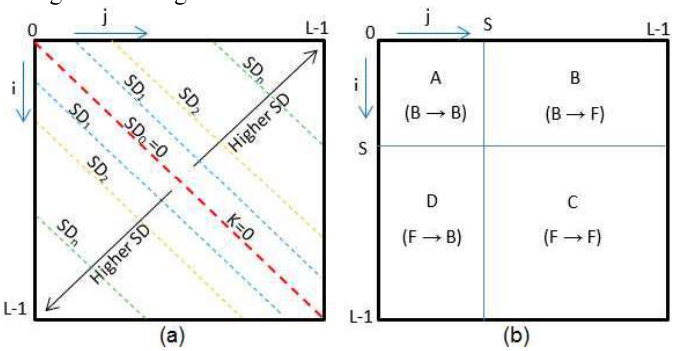

Fig 3 (a) Diagram of the SD distribution through the GLCM, (b) the four quadrants of the GLCM.

Although the object and background regions are two distinct regions in the image with distinct ranges of gray levels, they are not independent of each other, where knowledge of one can tell us about the likelihood of the other. Hence, the joint entropy (JE) thresholding method, proposed in [16], attempts to maximize the average amount of information that can be obtained from the object region considering knowledge about the background, and vice versa. This can be achieved by selecting a threshold value that maximizes conditional entropy of the object given the background ($H_{F \to B}$) along with conditional entropy of the background given the object ($H_{B \to F}$). Therefore, by using the joint quadrants from the GLCM, the threshold value S_{JE} is calculated as follows:

$$H_{joint}(s) = (H_{object \to background} + H_{background \to object} 3)$$

$$S_{JE} = \arg\left[\max_{s=0 \ldots L-1} H_{joint}(s)\right] \quad 4)$$

3.1 Wrist region segmentation

Accurate wrist region segmentation is a crucial step that ultimately supports proper ROIs localization. The joint entropy (JE) thresholding method has been used for wrist region segmentation since it is a GLCM-based thresholding method that exploits the inter-pixel spatial dependencies in the image. As a single global thresholding method, JE thresholding algorithm assumes that the image consists of only two regions, e.g. object and background, with distinct gray ranges in order to be able to calculate the optimal threshold that separates them. Figure 4 shows how accurate the JE detected the wrist region for different wrist images. From Figure 4.c1, it is obvious that the JE thresholding method accurately separates the wrist region from the background, by using the joint transitions between them.

On the other hand, the inaccurate segmentation in figures 4(c2-c3) arose because of the occurrence of flaws in the background region, as shown in figures 4(a2-a3). These flaws are considered extra regions with different properties, gray ranges and inter-pixel spatial correlations, causing deformation of the four quadrants of the GLCM by their gray transitions. Figures 4(b2-b3) show the resulting noisy GLCM, which leads to inaccurate threshold calculation. Therefore, these extra regions must be removed from the image before computing its GLCM. This guarantees satisfaction of the main assumption of single global thresholding and the GLCM purity before applying the JE thresholding method.

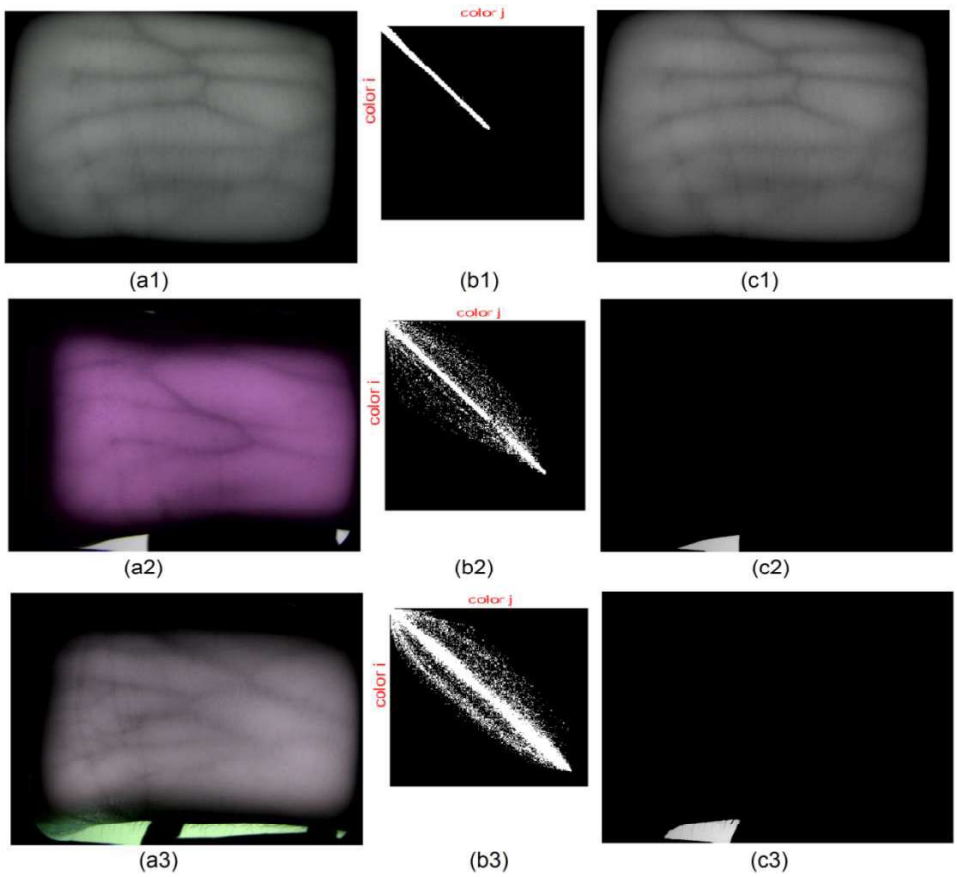

Fig 4

(a1-a3) wrist-vein images (b1-b3) top view of GLCM (c1-c3) detected regions using JE thresholding method

Let 'normal images' be the images that contain only two regions with distinct gray ranges, 'abnormal images' be those whose background has flaws, and 'noisy region' correspond to the region with the flaw. The GLCMs of the normal wrist images show that almost all gray transitions for both background and object regions are concentrated around the GLCM's primary diagonal line with high occurrence values as depicted in figure 5(b1, c1, d1). In the GLCMs of the abnormal wrist images, shown in figure 5(b2, c2, d2), it can be seen that there are many gray transitions that diffused across the GLCM with very small occurrences and much higher SD values. Let 'suspicious gray transitions' be the gray transitions that diffuse in the noisy GLCM with high SD and small occurrence, which are marked with red in figure 6.b.

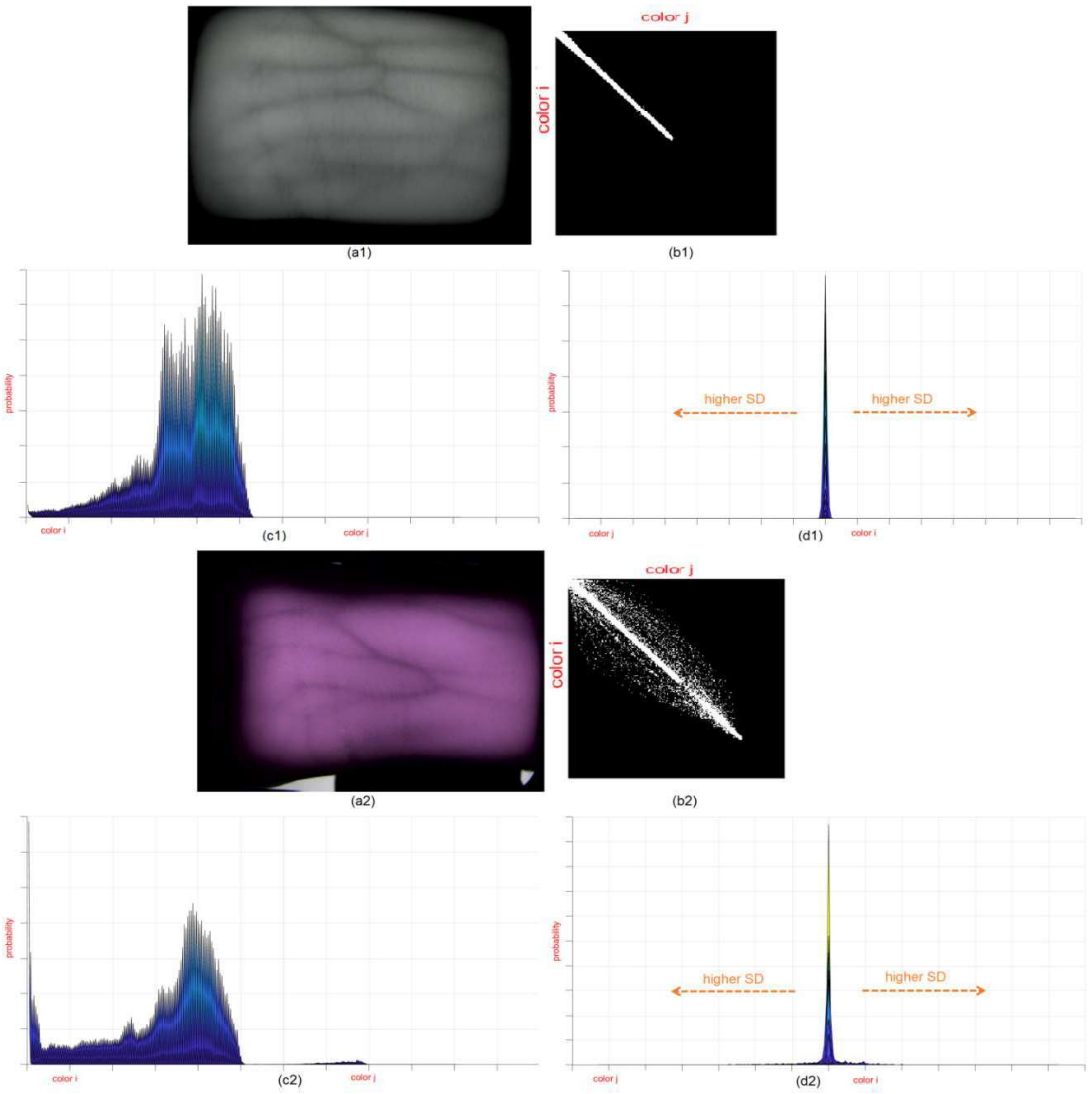

Fig 5 (a1-a2) wrist-vein images, (b1-b2) top view of the GLCM, (c1-c2) Left Side View of the GLCM, (d1-d2) Right Side View of the GLCM.

When the SD value between two adjacent pixels is very small, it means that their gray levels are close to each other and they belong to the same region in the image. In contrast, when the SD value between two adjacent pixels becomes higher, it means that there is a sharp gray transition between these pixels, and one of them might be an edge pixel between two different regions or just a noisy pixel. Based on these facts, when the suspicious gray transitions were re-projected to the image, it was found that most of them are corresponding to the edges of the noisy regions, as shown in Figure 6(c). Local and joint transitions of the flaw regions will have small number of occurrences compared to the occurrences of gray transitions belonging to the background and object regions, since these flaw regions have different inter-pixel spatial dependencies and they are smaller in size compared to the other two main regions in the image. It is worth noting that both joint transitions between the object and background regions and that between the noisy regions and another region in the image will have high SD values. Nonetheless, only the high SD values between adjacent pixels that faintly occurred in the image could be considered as the SD-values of the suspicious gray transitions, from which the edges of noisy regions can be detected.

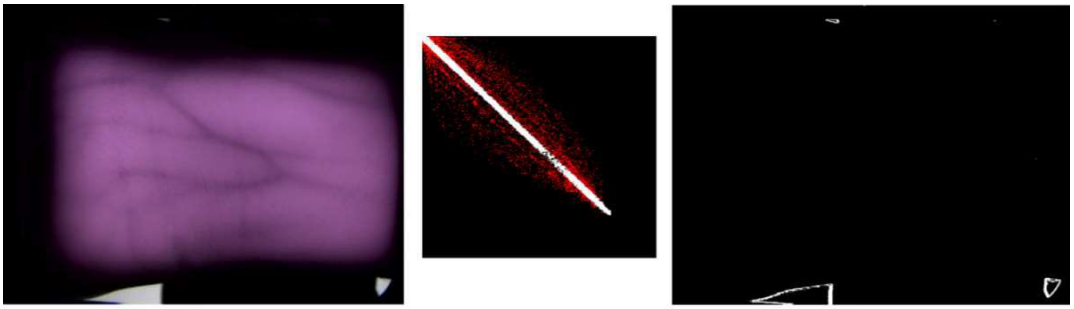

Fig 6 detection of noisy regions in a wrist image, (a) wrist-vein image, (b) GLCM with suspicious transitions in red, (c) detected edges of noisy regions

Therefore, the edges of the noisy regions can be detected by measuring the SD values for every pixel with each of its neighbors separately, considering only the horizontally right and vertically lower neighbors, then determining the high SD values that have small number of occurrences in the image. These SD values will be used for detecting the suspicious transitions in the image, by getting the adjacent pixels that produced these SD values between each other. The edge pixel in each suspicious gray transition is the pixel that causes more than one suspicious transition with its four neighbors including at least one suspicious transition at each region. Hence, a pixel belongs to the edges of noisy regions if it is common in at least two consecutive suspicious transitions. This means that, it must satisfy one or more of the transition cases shown in figure 7, where the red pixel is the edge pixel. Finally, by filling the areas inside these detected edges we can detect the whole noisy regions and delete them from the image before computing its GLCM.

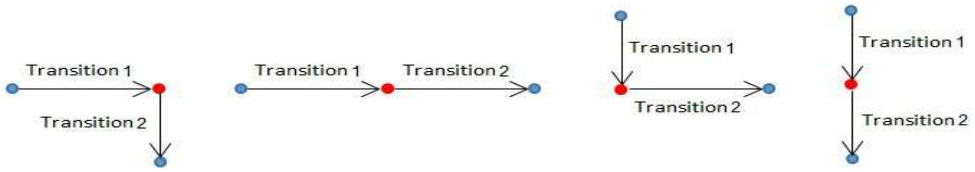

Fig 7 Four cases of two consecutive transitions

During the wrist images collection phase of the PUT vein database [20], which is used in this research, the volunteers were required to put his/her hand on the device to cover the whole acquisition window, cutting off external light sources. Thus, it was assumed that the wrist regions were illuminated in controlled stable lighting conditions with NIR uniform light. Unfortunately, covering the whole acquisition window condition wasn't satisfied in all images, since only a construction that allows placing palm and wrist in a convenient way was used without using an additional element that controls the hand position to ensure satisfying this condition. This led to the appearance, in some images, of the external lights in the surrounding space around the volunteer. In the images that the volunteer's wrist doesn't cover the whole acquisition window, most of the regions that appeared from the surrounding space seemed to be in green color. This means that some of the noisy regions are prevailed by green color, which may or may not be directly connected to the wrist region but they can't be considered as a part of the wrist region of interest, as shown in Figure 8.

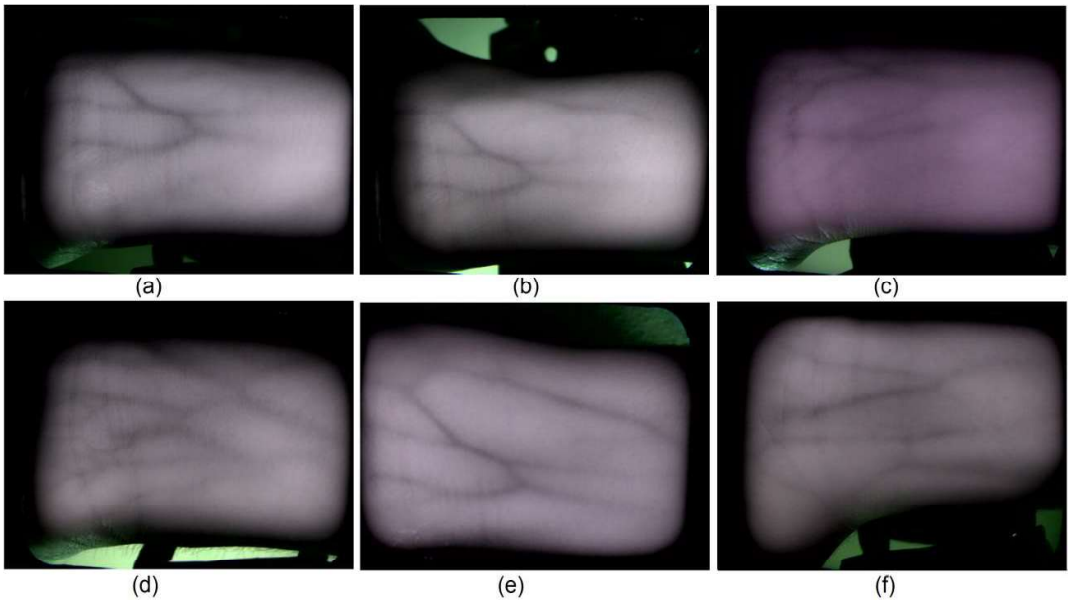

Fig 8 Examples of wrist images with green flaw regions in their backgrounds

Before converting the image into gray-scale image, any green color must be detected and removed in order to accelerate the wrist region segmentation algorithm and remove some of the useless data. Then, the proposed noisy regions detection approach must be applied on the gray-scale image to detect the remaining noisy regions and remove them before computing its GLCM. The green regions can be detected by two easy methods that were used together to complete each other. The first method determines the green color in an image by detecting those colors with green component higher than the other two components, while the second method defines the greenness of each pixel in the image by subtracting its gray scale image from its green channel. The whole green regions in the image can be detected by:

$$\mathrm{Greenness}_1(\mathrm{x},\mathrm{y}) = \mathrm{green}(\mathrm{x},\mathrm{y}) - \max(\mathrm{red}(\mathrm{x},\mathrm{y}), \mathrm{blue}(\mathrm{x},\mathrm{y})) \quad (5)$$

$$I_{green1}(x,y) = \mathrm{Greenness}_1(x,y) > T_1 \quad (6)$$

$$\mathrm{Greenness}_2(\mathrm{x},\mathrm{y}) = \mathrm{green}(\mathrm{x},\mathrm{y}) - \mathrm{gray}(\mathrm{x},\mathrm{y}) \quad (7)$$

$$\mathrm{I}_{\mathrm{green2}}(\mathrm{x},\mathrm{y}) = \mathrm{Greenness}_2(\mathrm{x},\mathrm{y}) > \mathrm{T}_2 \quad (8)$$

$$\mathrm{I}_{\mathrm{green}}(\mathrm{x},\mathrm{y}) = \mathrm{I}_{\mathrm{green1}}(\mathrm{x},\mathrm{y}) \mid \mathrm{I}_{\mathrm{green2}}(\mathrm{x},\mathrm{y}) \quad (9)$$

Where red, green, blue are the three channels of the original RGB image, while gray is its gray scale image. T_1 and T_2 are two predefined values that control the range of green colors that will be detected in the original image, producing the I_{green} binary image. Algorithm 1 presents the proposed wrist region segmentation algorithm. T_3 is predefined as the threshold for high SD values, and T_4 is predefined as the threshold for small occurrence values.

Algorithm 1 Proposed Wrist Region Segmentation
Input: I –original wrist-vein image Output: b –binary image of the segmented wrist region

```
for each wrist image (I) in the PUT dataset
    remove green colors
    calculate separately SD between each two adjacent pixels, in only the horizontally right &
vertically lower directions
    calculate occurrence of each SD value
    for each SD value
        if SD > T3 & its occurrence < T4
            list pixels pairs that produced this SD value as suspicious transitions
        end
    end
    for each pixel (p) in the suspicious transitions list
        if pixel (p) is common in at least two consecutive suspicious transitions
            list pixel (p) as an edge pixel along boundary of a noisy region
        end
    end
    fill areas inside the detected edges
    remove the detected regions
    compute the GLCM
    apply joint entropy thresholding
```

3.2 Wrist orientation correction

Allowing freely wrist positioning during image acquisition leads to random wrist posture deflections in different images for the same person. Therefore, the wrist orientation must be corrected by rotating it to the horizontal before localizing the ROI. By using the same approach used in [7,9,21] for finger orientation correction, the wrist orientation can be defined as the slope of the wrist central line. Hence, the wrist orientation can be corrected by rotating the image by an angle (ɵ) that is between the wrist central line and the horizontal line.

The wrist contour image denoted by C(x, y) is shown in figure 9.b. To obtain the wrist central line, the middle points between the upper and lower edge points in all columns having wrist contour points are calculated, to form an approximately straight line which represents the wrist central line. Thus, for each column y_i the corresponding x_i value of the wrist middle points can be defined as:

$$x_i = \frac{up_i + low_i}{2}, \quad i = 1,2,\ldots\ldots,n \qquad (10)$$

Where up_i and low_i are the x values of the upper and lower edge points on the i^{th} column respectively. For accurate wrist central line calculation, we have to neglect some columns from the left and right parts of the wrist contour in order to avoid the left and right wrist edges. As shown in figure 9.b, only the wrist edges between the two red lines will be used for the wrist central line calculation. This central line is fitted to a straight line using the least-squares estimation (LSE) method, in order to obtain its slope that is used for determining the direction and magnitude of the rotation angle (ɵ).

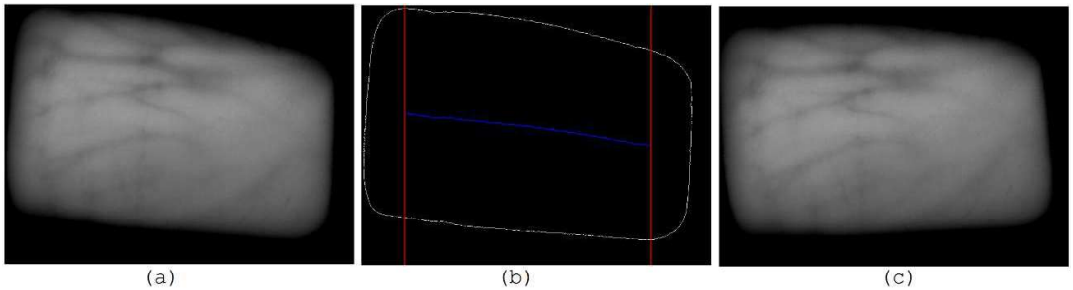

Fig 9 (a) wrist-vein image, (b) wrist region contour in white, estimated wrist central line in blue, (c) corrected wrist image

3.3 ROI detection

Many researches have defined the hand vein ROI as a rectangular region inside the detected hand region, in order to eliminate the background region and reduce the image size for reducing the computational cost of the vein recognition system subsequent steps. Even if the

ROI is considered to be the largest possible inner rectangular region that could be located inside the wrist region, shown as the red rectangle in figure 10.b, it may lead to losing some portions of the wrist vein structure. Therefore, in order to avoid this drawback, the whole detected wrist region has been considered to be the ROI and the image is cropped at the coordinates of the smallest possible outer rectangle that contains this region. Figure 10 shows the difference between the two ways of detecting ROI.

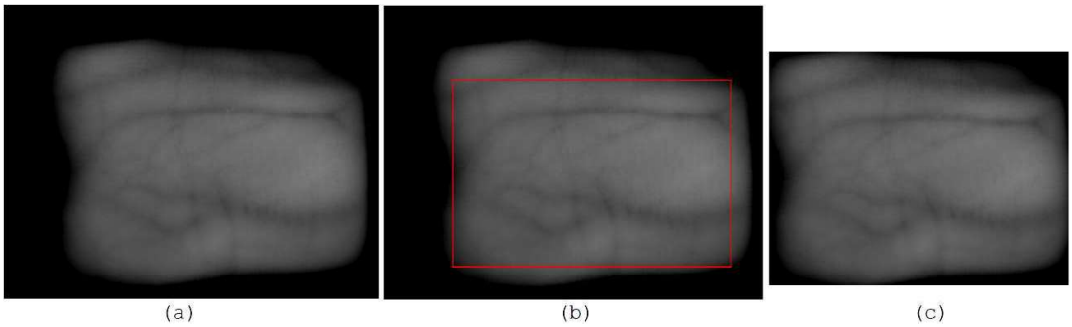

Fig 10 a) orientation corrected image, (b) ROI: largest inner rectangular region, (c) ROI: smallest outer rectangular region

4. EXPERIMENTAL RESULTS AND DISCUSSION

In order to examine the efficiency of the proposed segmentation method, it was necessary to compare its performance and processing time with other segmentation methods. Therefore, most of segmentation methods that have been used for hand region localization purpose in the vein pattern recognition researches (like finger vein, palm vein, dorsal vein, and wrist vein recognition researches), and other segmentation methods are implemented for comparison. All the 1200 wrist-vein images from the freely available PUT vein dataset have been used throughout our comparative analysis, which are 24-bit color images with a resolution of 1280*960 [20]. The wrist-vein images were acquired from both hands of 50 volunteers, resulting in 100 unique vein patterns for the wrist region. For each volunteer, for each hand, pictures were taken in 3 series, 4 pictures each, with at least one week interval between each series. Furthermore, all the experiments have been performed using MATLAB (R2017a) on Intel core i7 2.40 GHz laptop with 8 GB RAM.

For evaluating the performance of all the implemented segmentation methods, it was necessary to have a pre-defined wrist location in the dataset images to compare the output segmented images of each segmentation method with it. Therefore, we had to localize the wrist region in the images manually to be our ground-truth, by marking the boundaries of the wrist region for all wrist images in the PUT vein database.

The quality of segmented images has been measured by using six different evaluation metrics that can be classified into three categories: similarity metrics, distance metrics and popular classical metrics. The higher the values are for the similarity metrics and the lower the values are for the distance metrics, the better is segmentation performance. The Sensitivity (Recall, True Positive Rate) and Specificity (True Negative Rate) metrics haven't been used for segmentation evaluation. This is because the sensitivity can achieve its ideal value for a poor segmentation much bigger than the ground-truth, also the specificity can achieve its ideal value for a very poor segmentation that does not detect the object region at all. Thus, the accuracy metric can be more accurate and meaningful.

⇒ Similarity metrics:
1. Rand Index (RI)
2. Jaccard Similarity Coefficient (Tanimoto Coefficient)

⇒ Distance metrics:
3. Variations of Information (VOI)
4. Boundary Displacement Error (BDE)

⇒ Classic metrics:
5. Accuracy
6. Mean Square Error (MSE)

Table 2 shows the comparison between various segmentation methods for hand region localization in terms of performance and processing time. The second column to the

seventh column represent the performance recorded for each evaluation metric. The last column presents the average time, in seconds, required for each segmentation method to localize the wrist region in an image from the used dataset.

Table 2 Comparison between various segmentation methods in terms of performance and average processing time.

Technique	RI [0 1]	Jaccard [0 1]	VOI	BDE	Accuracy [0 100] %	MSE [0 1]	Time (sec)
Lee's region detection [5-7]	0.8874	0.9190	0.6097	17.161	93.945	0.0605	0.0270
Sobel edge detector [9-10]	0.9794	0.9857	0.1427	3.2971	98.961	0.0103	0.0551
Canny edge detector [11-12]	0.9862	0.9893	0.1082	1.6649	99.262	0.0073	0.1038
Otsu thresholding [13-15]	0.8382	0.8742	0.6766	25.534	91.079	0.0892	0.0219
K-means clustering [17-18]	0.8380	0.8740	0.6774	25.584	91.063	0.0893	0.3313

From table 2, it is shown that Otsu thresholding method produced low performance records, since there were big losses in the detected wrist regions due to non-fulfillment of the bimodal histogram condition in the used wrist images. The segmentation results of Canny and Sobel edge detectors suffered from connecting some unwanted background details to the wrist regions in images with complicated backgrounds, in addition to some tiny losses in the detected wrist regions due to some weak wrist edges. This caused decreasing their performance records. Lee's region localization produced low performance records due to occurrence of many of its weaknesses in most images. Hence, in spite of their speed, these segmentation methods have produced low performance records when the main assumption of each method was unsatisfied.

As a result of all these shortcomings, different segmentation methods have been tested on the wrist-vein dataset, all belonging to threshold-based segmentation techniques but they differ in how each one computes its threshold value. These thresholding methods are the IsoData thresholding, Min error thresholding (MET), Max entropy thresholding (ME), Min cross entropy thresholding (MCE), Local entropy thresholding (LE), Joint entropy thresholding (JE), Global entropy thresholding (GE), Local relative entropy thresholding (LRE), Joint relative entropy thresholding (JRE), and Global relative entropy thresholding (GRE).

Table 3 shows comparison of the performance and processing time for these segmentation methods. In the first column, thresholding methods are grouped according to their dependencies for computing their threshold values. The third column to the eighth column represent the performance recorded for each evaluation metric. The last column presents the average time, in seconds, required for each segmentation method to localize the wrist region in an image from the used dataset.

Table 3 Comparison between different thresholding methods in terms of performance and average processing time

Category	Technique	RI [0 1]	Jaccard [0 1]	VOI	BDE	Accuracy [0 100] %	MSE [0 1]	Time (sec)
Histogram-derived	IsoData	0.7788	0.8237	0.8422	36.903	87.308	0.1269	0.0287

thresholding methods	MET	0.9756	0.9828	0.1569	3.2232	98.751	0.0124	0.0505
	ME	0.5485	0.4396	1.2962	132.07	59.666	0.4033	0.0207
	MCE	0.9436	0.9587	0.3124	7.7549	97.088	0.0291	0.0324
Co-occurrence matrix derived thresholding methods	LE	0.5307	0.3188	1.2902	161.53	50.884	0.4911	0.2326
	JE	0.9811	0.9778	0.1140	4.8110	98.501	0.0149	0.2147
	GE	0.9533	0.9534	0.2390	9.7889	96.853	0.0314	0.2619
	LRE	0.6687	0.1841	0.7388	249.48	40.915	0.5908	0.2182
	JRE	0.9386	0.9212	0.2676	21.864	94.254	0.0574	0.2132
	GRE	0.6470	0.1217	0.7751	269.89	36.476	0.6352	0.1941
	Proposed method	0.9905	0.9933	0.0830	0.9555	99.524	0.0047	0.3119

From table 3, it can be seen that the IsoData, Min error thresholding (MET), Max entropy (ME), and Min cross entropy (MCE) thresholding methods produced low performance records. Since all of them depend only on the image's intensity histogram neglecting the dependencies between the pixel intensities in the image and its spatial information, it was necessary to use other thresholding methods that compute their threshold values in different way in order to overcome this weakness point. Therefore, the co-occurrence matrix based thresholding methods have been included in our comparison so as to examine their effectiveness for segmenting the wrist region in the used NIR dataset.

From experiments, it was found that the joint-entropy thresholding technique has produced higher performance records than the other GLCM-based thresholding techniques, as shown in table 3. However, its performance results have been affected due to its failures in the images containing flaws in their backgrounds. By applying the proposed segmentation algorithm, the segmentation results have become more accurate, because of removing the noisy regions from these images and ensuring their GLCM purity before applying the JE thresholding method. Accordingly, it can be seen that the proposed segmentation method has produced the highest RI and Jaccard records, and the lowest VOI and BDE records, while producing 99.524% accuracy that is 1.022% more accurate than the original JE thresholding method.

Figure 11 shows three wrist-vein images with noisy regions in their backgrounds, being segmented using JE thresholding method and the proposed segmentation method. The red lines show the segmentation by JE thresholding method, while the blue lines define the segmented region using the proposed segmentation method. It is obvious that in the first two images, the JE method didn't detect the wrist region at all but it detected the noisy regions in the background instead. In the last image, the JE output included the noisy regions in the background as a part of the detected wrist region. In contrast, the proposed segmentation method is able to accurately detect the wrist region in these noisy images.

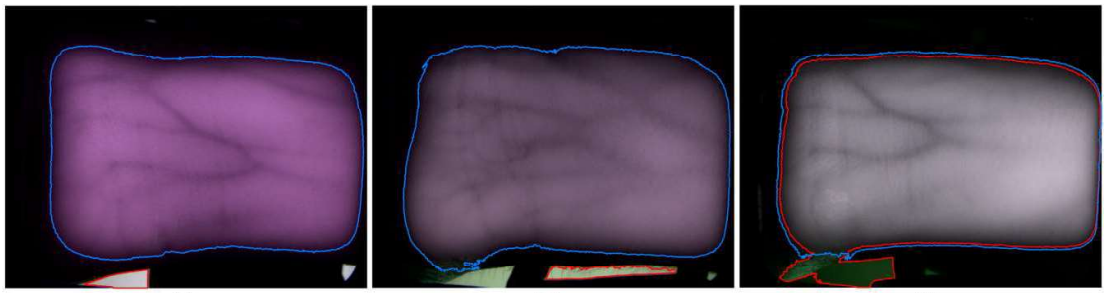

Fig 11 Segmentation of wrist images with noisy regions: red line denotes JE thresholding method, blue line denotes the proposed method.

5. CONCLUSION

In this paper, a wrist-vein ROI localization algorithm has been proposed that consists of three steps: wrist region segmentation, wrist orientation correction and ROI detection. JE thresholding method has been used for wrist region segmentation, since it depends on a higher-order statistic of the image that considers its local spatial correlations by using its GLCM instead of relying only on the image global characteristics. Existence of more than two regions in the acquired image due to flaws during capturing causes a deformation of its GLCM resulting in inaccurate threshold calculation. Therefore, a pre-processing step has been proposed to eliminate the useless noisy regions from the image, in order to guarantee the GLCM purity before applying the JE thresholding method. After wrist region segmentation, the orientation of the detected wrist region is estimated in order to be corrected. Finally, the wrist-vein ROI has been defined as the smallest possible rectangular region that can contain the whole wrist region, in order to accelerate the subsequent steps of the vein recognition system without losses in the veins structure.

Experiments show that the proposed segmentation algorithm has produced 1.022% more accurate wrist region segmentation results than using joint-entropy thresholding method by its own, producing totally an accuracy of 99.524%. Moreover, it is applicable for real-time wrist-vein recognition systems, requiring average processing time 0.321 sec for a wrist image.

In the future, we will dedicate our efforts to build an integrated wrist-vein recognition system to examine the efficiency of using wrist veins for individual recognition.

REFERENCES

[1] Jain, A., Bolle, R., and Pankanti, S.- 1999- "Biometrics personal identification in networked society"- (Kluwer, Boston, MA, USA)

[2] Lingyu Wang and Graham Leedham- 2006- "Near- and Far- Infrared Imaging for Vein Pattern Biometrics", Proceedings of the IEEE International Conference on Video and Signal Based Surveillance (AVSS'06)

[3] Dat Tien Nguyen, Hyo Sik Yoon, Tuyen Danh Pham, and Kang Ryoung Park- 2017- "Spoof Detection for Finger-Vein Recognition System Using NIR Camera", Sensors

[4] Daniel Kocher, Stefan Schwarz, and Andreas Uh- September 2016- "Empirical evaluation of LBP-extension features for finger vein spoofing detection", In Proceedings of the International Conference of the Biometrics Special Interest Group, Darmstadt, Germany, 21–23; pp. 1–5.

[5] Eui Chul Lee, Hyeon Chang Lee, Kang Ryoung Park- September 2009- "Finger Vein Recognition Using Minutia-Based Alignment and Local Binary Pattern-Based Feature Extraction", International Journal of Imaging Systems and Technology

[6] Marios Vlachos, Evangelos Dermatas- 2015- "Finger Vein Segmentation from Infrared Images Based on a Modified Separable Mumford Shah Model and Local Entropy Thresholding", Computational and Mathematical Methods in Medicine

[7] JiaLiang Peng, Qiong Li, Ning Wang, Ahmed A. Abd El-Latif, and Xiamu Niu- 2013- "An Effective Preprocessing Method for Finger Vein Recognition", Fifth International Conference on Digital Image Processing (ICDIP), SPIE

[8] Yu Lu, Shan Juan Xie, Sook Yoon, Jucheng Yang, and Dong Sun Park- 2013- "Robust Finger Vein ROI Localization Based on Flexible Segmentation", Sensors

[9] Lu Yang, Gongping Yang, Yilong Yin and Rongyang Xiao- 2013- "Sliding Window-Based Region of Interest Extraction for Finger Vein Images", Sensors
[10] Lizhen Zhou, Gongping Yang, Yilong Yin, Lu Yang, and Kuikui Wang- 2016- "Finger Vein Recognition Based on Stable and Discriminative Superpixels", International Journal of Pattern Recognition and Artificial Intelligence Vol. 30, No. 6
[11] Randa Boukhris Trabelsi, Alima Damak Masmoudi, Dorra Sellami Masmoudi- 2014- "Hand vein recognition system with circular difference and statistical directional patterns based on an artificial neural network", Springer Science+Business Media New York
[12] M. Khalil-Hani, P.C. Eng- 2011- "Personal Verification using Finger Vein Biometrics in FPGA-based System-on-Chip", ELECO 7th International Conference on Electrical and Electronics Engineering, 1-4 December, Bursa, TURKEY
[13] Wee Lorn Jhinn, Goh Kah Ong Michael, Tee Connie and Liew Tze Hui- 2015- "Preliminary Work on Rotation-Invariant Algorithms for Contactless Palm Vein Biometrics", 3rd International Conference on Information and Communication Technology (ICoICT)
[14] R. Raghavendra, Jayachander Surbiryala, Christoph Busch- 2015- "An efficient finger vein indexing scheme based on unsupervised clustering", IEEE, International Conference on Identity, Security and Behavior Analysis (ISBA)
[15] M.Rajarajeswari, G.Ashwin- May 2014- "Dorsal Hand Vein Authentication Using FireFly Algorithm And Knuckle tip Extraction", 4th National Conference on Advanced Computing, Applications & Technologies
[16] N. R. Pal and S. K. Pal- 1989- "Entropic thresholding", Signal Process, 16, pp. 97–108
[17] Seyed Mehdi Lajevardi, Arathi Arakala, Stephen Davis, Kathy J. Horadam- 2014- "Hand vein authentication using biometric graph matching", The Institution of Engineering and Technology
[18] V.H.Yadav, Prof.S.O.Rajankar- 2012- "Dorsal Hand Vein Biometry by Independent Component Analysis", International Journal on Computer Science and Engineering (IJCSE)
[19] Hong Yao, Qingling Duan, Daoliang Li, Jianping Wang- 2013- "An improved K-means clustering algorithm for fish image segmentation", Mathematical and Computer Modelling
[20] Vein Pattern Dataset (VPD), CIE Biometrics, URL: http://biometrics.put.poznan.pl/vein-dataset/
[21] Chunting Zuo, Kejun Wang, and Xinjing Song- 2013- "A New ROI Extraction Method of Non-contact Finger Vein Images", Springer